THE ASTROPHYSICAL JOURNAL, 227:450–465, 1979 January 15

TYPE I OH MASERS: A STUDY OF POSITIONS, POLARIZATION, NEARBY WATER MASERS, AND RADIO CONTINUUM AND INFRARED PROPERTIES

NEAL J. EVANS II*†
Owens Valley Radio Observatory, California Institute of Technology; and
Department of Astronomy, The University of Texas at Austin

S. BECKWITH
California Institute of Technology

ROBERT L. BROWN
National Radio Astronomy Observatory

AND

W. GILMORE
University of Maryland

Received 1978 May 10; accepted 1978 August 2

ABSTRACT

A study of 11 type I OH masers is presented. We have determined the maser positions with the Owens Valley interferometer to an accuracy of $\pm 5''$. Stokes parameters of the emission features are given; several masers show strong linear polarization. H_2O masers were detected in the directions of eight of the sources. Radio continuum observations at 2695 and 8085 MHz were made with the NRAO interferometer; six of the OH masers are coincident with compact H II regions which are optically thick at 2695 MHz. Infrared observations toward the positions of OH masers have resulted in the discovery of seven new infrared sources at 10 μm. Infrared photometry of these sources is presented.

The spatial coincidences of OH masers, compact H II regions, infrared objects, and H_2O masers are examined. The strongest correlation is found between OH and H_2O masers, but this effect may be due to the large uncertainties in the H_2O maser positions. The correlation of infrared objects with OH masers is about as strong as the correlation of compact H II regions with OH masers. The data are used to test several proposed pump models for each maser, those which pump the OH maser by ultraviolet photons, far-infrared photons, and anisotropic collisions. Quite generous assumptions are required in order to predict enough ultraviolet or far-infrared photons to produce the observed flux of maser photons. The model with anisotropic collisions predicts sufficient fluxes, but its theoretical basis is incomplete.

Subject headings: infrared: sources — interferometry — masers — nebulae: general — polarization

I. INTRODUCTION

OH masers which emit predominantly at 1665 MHz (type I in the notation of Turner 1970*a*) appear to be associated with young objects in regions of recent star formation, but neither the pump mechanism nor the precise nature of the masing region has been conclusively established. Habing *et al.* (1974) have found a relatively strong correlation between 1665 MHz OH masers and the presence of a compact H II region. They suggested that such an H II region is necessary for type I maser emission. Their study and most earlier studies of OH sources are biased toward OH masers near well-developed H II regions. It is thus difficult to decide whether infrared sources or compact H II regions are causally related to the OH masers.

The surveys of Turner (1970*b*), Downes (1970), Robinson, Caswell, and Goss (1971), and Turner (1978) discovered a large number of 1665 MHz masers; these provide a larger and less biased sample for study. In particular, the survey of Turner (1978) is not biased toward known H II regions within the zone of $|b^{II}| \leq 1°$ and $337° \leq l^{II} \leq 85°$. We have measured positions for 11 of the OH masers from this survey. These 11 masers represent a random sample of those found by Turner. A number of additional masers were studied at infrared wavelengths to check the connection between OH masers and infrared sources.

II. OBSERVATIONS

Observations were made with the Owens Valley 130 foot (40 m) telescope to establish approximate positions of the OH masers. The 100-channel autocorrelator was used with a resolution of 2.5 kHz or 0.45 km s^{-1}. This system was also used with a resolution of 0.625 kHz (0.11 km s^{-1}) to resolve lobe

* Guest Investigator at the Hale Observatories.

† Visiting Astronomer, Kitt Peak National Observatory, which is operated by the Association of Universities for Research in Astronomy, Inc., under contract with the National Science Foundation.

ambiguities present in the interferometer data and to obtain Stokes parameters.

The OH position measurements were made during 1974 May–June with the Owens Valley interferometer arranged in a north-south baseline of 244 meters. The observing procedure and system parameters were described by Evans, Crutcher, and Wilson (1976); a bank of 23 filters of 1 kHz width was added in parallel to 24 of the 4 kHz filters. Two local oscillator settings were used, so that the 1 kHz filters provided 0.18 km s^{-1} resolution over a range of 6.3 km s^{-1}. Because most of the sources have only a few velocity features, this range provided sufficient velocity coverage. The rms noise in a single 1 kHz channel was 1 Jy in a typical 10 minute integration. The flux calibration was determined by interpolating the tabulated fluxes of calibrators to 1665 MHz.

The baseline was determined to 1.4% (1% of phase variation $\sim 1''.8$) by observing 20 unresolved continuum sources over a wide range of declinations and hour angles. The instrumental phase and gain were calibrated about once per hour on nearby continuum sources. The fit to the instrumental phase was good to 1%, and the fit to the gain was good to 10%. The total phase variation was generally less than 3% during a day, but was 6% on 1 of the 4 days. We have assigned a minimum uncertainty of $\pm 5''$ in each coordinate to allow for systematic effects of this sort.

The 130 foot telescope was used in 1975 June–July to search for H_2O masers at the positions of the OH masers. Observations were made with resolutions of 25 kHz (0.34 km s^{-1}), 6.25 kHz (0.08 km s^{-1}) and 2.50 kHz (0.03 km s^{-1}). The system temperature was $\sim$700 K, the aperture efficiency was $\sim$25% ($\sim$9 Jy per K of antenna temperature), and the half-power beamwidth was $\sim 95''$.

The radio continuum observations were carried out with the three-element interferometer at the National Radio Astronomy Observatory[1] operated at frequencies of 2695 and 8085 MHz. For each of the radio observations, a single telescope-pointing position, centered on the position of the OH emission source, was used; this technique enabled us to search for radio continuum emission over a region 18′ in diameter at 2695 MHz and 6′ in diameter at 8085 MHz. The purpose of the radio continuum observations was to determine the positions, sizes, and fluxes of any sources which existed in the fields searched; no attempt was made to obtain complete synthesis maps. The interferometer baselines used for these observations were 200, 300, 600, 900, 1500, 1800, 1900, 2100, and 2700 m, although not all of the OH positions were observed at both frequencies on all baselines. For each of the observed regions, maps were constructed at both frequencies; where sources were present, one or more elliptical Gaussian components were fitted to the calibrated data. Owing to our incomplete (u, v) coverage, these observations are not uniformly sensitive to continuum emission on all angular scales. In particular, the absence of very short spacings in the observations severely restricts the sensitivity to extended emission. This problem is most acute at 8085 MHz. Hence these observations are useful in establishing the radio continuum properties of only the more compact components present in each field, those with angular diameters $\lesssim 15''$ at 2695 MHz and $\lesssim 6''$ at 8085 MHz.

[1] Operated by Associated Universities, Inc., under contract with the National Science Foundation.

Most of the infrared observations were made with the 60 inch (1.5 m) telescope at Mount Wilson Observatory and the system described by Beckwith *et al.* (1976). Observations were made with a spatial resolution of 9″ (FWHM) and a beam separation of 13″ for sky subtraction. Standard stars were observed periodically for the purposes of calibration and standard air-mass corrections were applied to the measurements. For measurements made at 2.2 μm, 3.4 μm, 4.8 μm, and 10 μm, the uncertainties result mainly from statistical uncertainties; for measurements made at 8.7 μm, 9.5 μm, 11.2 μm, 12.5 μm, and 20 μm, the uncertainties result mainly from uncertainties in the system calibration and air-mass corrections. The aperture was positioned spatially by guiding with an offset eyepiece on nearby field stars whose positions were measured to $\pm 1''$ from the Sky Survey plates. The actual position uncertainties are of order 5″; they are due to guiding errors and uncertainties in peaking up weak sources. The infrared source associated with NGC 2071 was observed at 3.4 and 2.2 μm with a spatial resolution of 30″ and a beam separation of 60″ at the 1.3 m telescope of the Kitt Peak National Observatory. The observing technique is described by Evans, Blair, and Beckwith (1977).

For the OH source positions at which infrared upper limits are given, five measurements were made, one measurement at the source position and four measurements at positions displaced by half the diameter of the aperture north, south, east and west of this position. The quoted limits are the largest limit of these measurements in each case. All the limits are 3 standard deviations.

III. RESULTS

a) *Positions*

The positions of the OH masers are presented in Table 1. The positions of different velocity features agree within the uncertainties. Only the data from the 1 kHz filters have been used to determine the positions in Table 1, although the positions determined from the 4 kHz filters agree very well. The position of OH 19.6−0.2, which was measured by Goss *et al.* (1973), was remeasured as a check and agreed well. Caswell and Robinson (1974) used the Parkes 210 foot (64 m) telescope to measure a position for OH 353.4−0.3 with $\sim 30''$ errors. The position of OH 353.4−0.3 in Table 1 is $\sim 3'$ east of their position. Because no lobe-shifted positions are possible within 13′ east or west of the position in Table 1, it is probably correct. For OH 355.2+0.1, a lobe-shifted position is possible $\sim 7'.5$ north and 1′ west of the position in Table 1.

b) *Polarization*

Table 2 presents the Stokes parameters of the OH masers for each identifiable velocity feature. The

TABLE 1

OH POSITIONS

Source (1)	α(1950) (2)	δ(1950) (3)	Velocity† (km s^{-1}) (4)	Peak Flux† (Jy) (5)	References (6)
OH353.4-0.3	$17^h27^m05^s.9\pm14''$	$-34°39'26''\pm5''$	-20.6	5	2, 3, 4
			-19.6	5	
OH355.2+0.1	17 30 12.0±8	-32 45 54 ±5	16.3	11	2, 3
			18.5	12	
			19.6	9	
OH12.2-0.1	18 09 48.2±6	-18 25 13 ±5	27.6	22	6
			28.8	23	
OH12.9-0.3	18 11 43.9±5	-17 52 57 ±5	36.5	83	6, 8
			37.3	44	
			38.0	69	
			39.7	130	
OH19.6-0.2	18 24 50.4±16	-11 58 24 ±6	41.8	3	2, 3, 4, 5
OH34.3+0.2	18 50 46.5±5	+01 11 16 ±5	55.7	19	3
			58.0	49	
			59.0	29	
OH35.2-1.7	18 59 12.5±5	+01 09 16 ±5	42.1	49	6
			43.6	9	
			44.8	10	
OH35.6-0.0	18 53 51.7±5	+02 16 31 ±5	48.9	52	1, 2, 3, 4
OH40.6-0.1	19 03 34.9±6	+06 41 55 ±5	32.3	62	6
OH43.8-0.1	19 09 30.5±7	+09 30 46 ±5	38.8	14	6, 7
			41.3	125	
			43.3	9	
OH48.6+0.0	19 18 13.0±5	+13 49 46 ±5	19.7	15	2, 4
			20.4	14	

NOTES TO TABLE 1

† For sources with multiple velocity features, the velocity and peak flux of each feature are given.

REFERENCES.—(1) Downes 1970. (2) Turner 1970*b*. (3) Dickinson and Turner 1972. (4) Caswell and Robinson 1974. (5) Goss *et al.* 1973. (6) Turner 1978. (7) Winnberg *et al.* 1975. (8) Wynn-Williams, Werner, and Wilson 1974.

fractions of linear (P_L) and circular (P_C) polarization are also given in Table 2. Many of the features show large (> 0.90) circular polarizations. A surprising result is that several features exhibit large linear polarization. For comparison, only one of 50 features recorded by Palmer and Zuckerman (1967) exhibits linear polarization; this feature is in W75 ($P_L = 0.42$). Most of the sources studied by Palmer and Zuckerman are associated with large H II regions and displayed many velocity components. Two of the sources in Table 2 with large linear polarization have only a single, very narrow velocity feature, and a third source has only two velocity features. These facts suggest that linear polarization becomes apparent in sources with simple velocity structures.

The uncertainties in the entries in Table 2 arise from statistical uncertainties, differences in the system response at different polarization angles, and insufficient velocity resolution. The statistical uncertainties in all four Stokes parameters are ± 3 Jy. Upper and lower limits on S_3 are used to indicate that no feature with $S_v > 3$ Jy could be detected in one circular polarization. These limits are translated into lower limits on P_C. The uncertainties in P_L and P_C are calculated from the statistical uncertainties. The errors in the Stokes parameters introduced by differing system response to different polarization angles may be estimated from the values of total flux given in columns (2)–(4). These were derived from three different pairs of polarizations, as described in the notes to Table 2. Averaging over all features gives $\langle S_0'/S_0 \rangle = 1.05 \pm 0.13$ and $\langle S_0/S_0'' \rangle = 1.12 \pm 0.11$; ideally these would all be equal. Thus the only possibly significant *systematic* difference in the Stokes parameters is between circular and linear polarizations. Nonetheless, an average of S_0 and S_0' has been used to determine P_L. An additional uncertainty arises because many of the features are extremely narrow (col. [11] of Table 2) and the lines could not be centered in exactly the same way at each polarization. The effect of this uncertainty can be seen in Table 2. The differences between the individual entries in columns (2)–(4) exceed those expected from statistical uncertainties in many cases. For this reason, the Stokes parameters for OH

TABLE 2

POLARIZATION MEASUREMENTS

Source (1)	S_o (Jy) (2)	S'_o (Jy) (3)	S''_o (Jy) (4)	S_1 (Jy) (5)	S_2 (Jy) (6)	S_3 (Jy) (7)	P_L (8)	P_C (9)	V (km s^{-1}) (10)	ΔV (km s^{-1}) (11)
OH12.2-0.1	56	54	45	2	8	>42	0.15±0.05	≥0.93	28.1	0.4 s
	52	57	46	-2	-3	-10	0.07±0.06	0.22±0.07	29.4	0.6 s
OH12.9-0.3*	32	27	26	2	-5	<-21	0.18±0.10	>0.81	35.6	0.4
	78	61	50	6	-3	30	0.10±0.04	0.60±0.07	37.4	- s
	149	146	148	60	-46	0	0.51±0.02	0.00±0.02	37.8	0.3 s
	133	118	114	45	-18	66	0.39±0.02	0.58±0.03	38.6	0.4 s
	231	226	234	-31	10	-182	0.14±0.01	0.78±0.01	40.3	0.6 s
OH34.3+0.2	45	41	44	3	5	≤-36	0.14±0.07	≥0.82	56.2	0.5
	111	103	93	19	15	53	0.23±0.03	0.57±0.04	58.6	0.4 s
	107	80	105	-3	2	73	0.03±0.03	0.70±0.03	58.7	0.4 s
	57	55	50	5	1	≥46	0.09±0.05	≥0.92	59.5	0.3
OH35.2-1.7	90	101	86	-16	-19	-70	0.26±0.03	0.81±0.04	42.1	0.4 s
	51	51	45	11	13	≤-41	0.33±0.06	≥0.91	42.9	- s
	29	32	29	-5	6	≤-26	0.26±0.11	>0.90	44.0	0.4
	26	20	23	6	-2	<-21	0.27±0.12	>0.87	45.5	0.4
OH35.6-0.0	107	100	92	41	-48	16	0.61±0.03	0.17±0.03	49.4	0.3
OH40.6-0.1	169	172	162	-63	48	-68	0.47±0.02	0.42±0.02	32.9	0.4 s
OH43.8-0.1	30	24	21	-2	+2	<-18	0.10±0.10	>0.86	39.4	0.5 s
	104	96	105	8	0	-31	0.07±0.03	0.30±0.03	41.5	0.4 s
	306	289	274	-52	74	-72	0.30±0.03	0.27±0.01	41.9	0.4 s
OH48.6+0.0	46	50	-	-8	-11	-	0.29±0.07	-	20.2	0.5
	50	52	-	-6	-34	-	0.68±0.07	-	20.9	0.4

Notes to Table 2

$S_o = S_\nu(0°) + S_\nu(90°)$, $S'_o = S_\nu(45°) + S_\nu(135°)$, $S''_o = S_\nu(RC) + S_\nu(LC)$

$S_1 = S_\nu(0°) - S_\nu(90°)$, $S_2 = S_\nu(45°) - S_\nu(135°)$, $S_3 = S_\nu(RC) - S_\nu(LC)$

$$P_L = \frac{(S_1^2 + S_2^2)^{0.5}}{0.5(S_o + S'_o)}, \quad P_C = \frac{|S_3|}{S''_o}$$

*OH12.9-0.3 has a particularly complex spectrum, and the Stokes parameters may be affected by line blending.

40.6−0.1 were derived from an average over three channels. This procedure causes an underestimate of S_0, but decreases the errors introduced in the other Stokes parameters. Multiple, blended features (marked by an *s* in col. [11]) are certainly present in several sources and may be present even in the apparently simple spectra. Examples of a "complex" spectrum and a "simple" spectrum are shown in Figure 1.

c) H_2O *Emission*

The measurements of the H_2O masers are presented in Table 3. H_2O emission was detected in all eight sources searched; the range of velocities of the H_2O maser features agrees well with that of the OH masers, although the individual features do not correspond in detail. Several of these sources have been detected in other searches. In addition to the sources listed in Table 3, H_2O maser emission has been seen toward OH 19.6−0.2 at a velocity near that of the OH (Lo, private communication). The discovery (Johnston, Sloanaker, and Bologna 1973) of the H_2O maser toward OH 35.6−0.0 showed emission at 58 and 64.2 km s^{-1}, while our spectrum shows emission only at 44.9 km s^{-1}. In the cases of H_2O 34.3+0.2, H_2O 35.2−1.7, and H_2O 48.6+0.0, the velocities in our spectra are in reasonable agreement with those in previous spectra.

d) *Radio Continuum Results*

The results of the radio continuum observations are presented in Table 4. A number of points regarding the radio components given in this table deserve mention. First, the table includes the parameters of all the compact radio sources present in the observations, not just those at or near the OH emission sources. Second, the absence of very short spacings at 8085 MHz is reflected in the fact that, at this frequency, the largest radio components present in the 2695 MHz

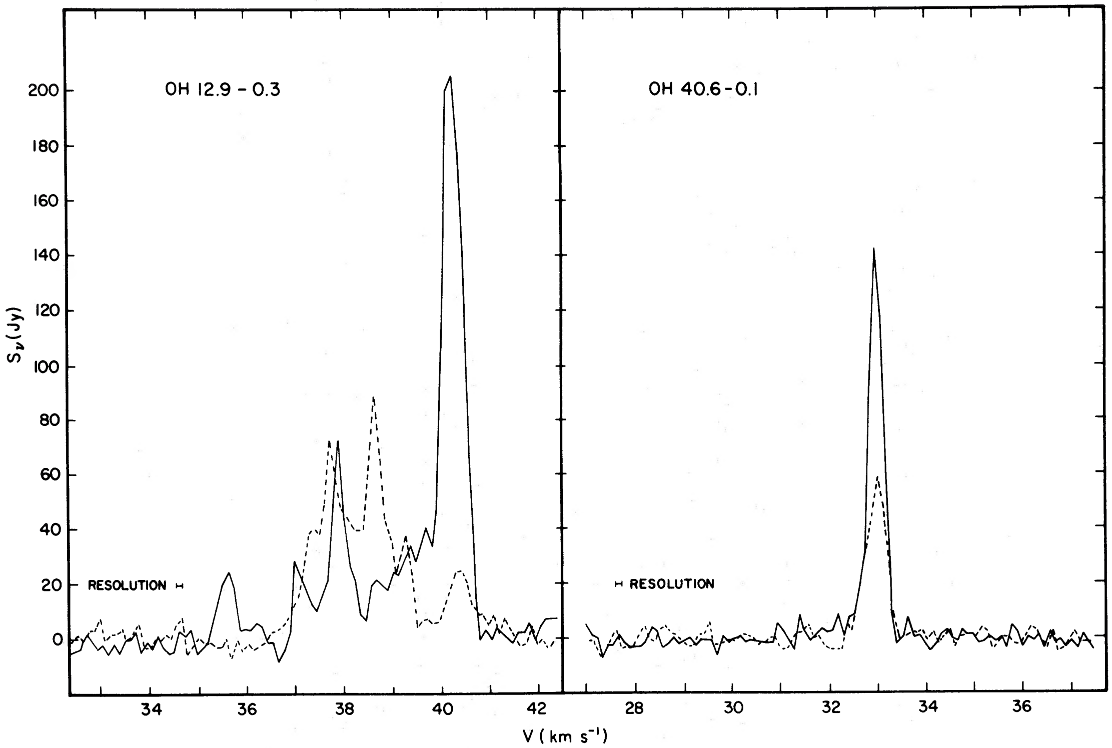

FIG. 1.—Spectra of a "simple" OH maser, OH 40.6−0.1, and of a "complex" OH maser, OH 12.9−0.3. The solid line indicates right circular polarization, and the dashed line indicates left circular polarization.

TABLE 3

H_2O MASERS

Source (1)	T_A (K) (2)	V (km s^{-1}) (3)	ΔV (km s^{-1}) (4)	V_{RANGE} (km s^{-1}) (5)	References (6)
OH12.2-0.1	6	24.7	0.7	12-44	
OH12.9-0.3	1.4	37.0	1.0	22-52	
OH34.3+0.2	8	55.8	1.7	40-70	
	43	60.1	0.7		1,2
OH35.2-1.7	2.0	44.8	0.6	27-57	3
	3.3	46.4	0.4		
OH35.6-0.0	8	44.9	2.0	33-64	4
OH40.6-0.1	3	34.6	0.6	17-47	
OH43.8-0.1	26	38.2	0.8	25-56	
	34	39.7	0.9		
	140	41.2	1.2		
OH48.6+0.0	3.0	16.8	0.5	5-35	4
	2.3	24.7	0.9		

1) Turner and Rubin 1971
2) Caswell et al. 1974
3) Lo, K. Y., private communication
4) Johnston, Sloanaker, and Bologna, 1973

TABLE 4

RADIO CONTINUUM OBSERVATIONS OF COMPACT H II REGIONS AT THE POSITIONS OF THE OH EMISSION SOURCES

Source (1)		Freq (2)	α(1950)* (3)	δ(1950)* (4)	Ang. dia.** (arc sec) (5)	Flux Density+ (mJy) (6)	Coincident with OH? (7)	Notes (8)
OH353.4−0.3	a)	2695	$17^h27^m07\overset{s}{.}8$	−34°39'29"	12	2450±150	No	1
		8085	" " 07.0	" " 33	>8.5	>600	No	
	b)	2695	17 27 06.5	−34 39 28	2.5	230±40	Yes	
		8085	" " 06.5	" " 27	2.5	800±70	Yes	
OH355.2+0.1		2695	17 30 12.5	−32 45 54	3.8	410±20	Yes	2
		8085	" " "	" " 55	4.2	670±40	Yes	
OH12.2−0.1		2695	18 09 43.8	−18 25 13	7.5	320±30	No	3
		8085	" " 43.7	" " 11	6.8	525±70	No	
OH12.9−0.3		2695	18 11 24.8	−17 55 09	>13	>5000	No	4
		8085	No high brightness radio continuum components			<20		
OH19.6−0.2	a)	2695	18 24 50.4	−11 58 31	7.5	2100±100	Yes	5
	b)	2695	18 24 50.7	−11 58 30	4.2	800±60	Yes	
		8085	" " 50.9	" " 26	3.6	725±60	Yes	
OH34.3+0.2		2695	18 50 46.2	+01 11 09	<6	840±100	Yes	6
		8085	" " 46.0	" " 14	1.6	1350±90	Yes	
OH35.2−1.7		2695	18 59 13.9	+01 09 03	<8	1180±190	No	7
		8085	" " 14.0	" 08 45	1.8	380±40	No	
OH35.6−0.0		2695	18 53 51.4	+02 16 29	<3	90±15	Yes	8
		8085	" " 51.3	" " 31	1.9	130	Yes	
OH40.6−0.1		2695	No Radio Continuum Emission			<15		
		8085	No Radio Continuum Emission			<15		
OH43.8−0.1	a)	2695	19 09 31.4	+09 30 49	<3	12±3	Yes	9
		8085	" " 30.9	" " 47	1.0	58	Yes	
	b)	2695	19 09 29.3	+09 30 46	15	>110	No	

*Errors on the quoted positions result both from the observational uncertainties and from the source modeling procedure as discussed in the text. Typical errors are ≲3" in each coordinate at 2695 MHz and ~1" in each coordinate at 8085 MHz.

**Quadratic mean of the FWHM dimensions of the best-fit elliptical Gaussian.

+Total flux density of the compact components, θ≲10". For more extended structures this is the maximum observed fringe amplitude.

NOTES TO TABLE 4

[1] OH 353.4−0.3 is seen toward a bright (7 Jy at 2695 MHz), 2′ × 3′ H II region (Altenhoff *et al.* 1970). The larger radio component in Table 2 refers to this region but it is easily resolved by our observations. At 8085 MHz the extended component is heavily resolved.

[2] The radio continuum from the region of OH 12.2−0.1 has also been studied at 6 and 21 cm by Shaver and Danks (1978). They also find that the compact source does not agree with the OH maser position, but they do find a ridge of weak continuum emission which overlaps the OH position.

[3] OH 355.2+0.1 is 7′ north of NGC 6383, a low-surface-brightness 15 Jy H II region.

[4] OH 12.9−0.3 is near, but not coincident with, W33, which we see heavily resolved at 2695 MHz. Our limit to the radio emission from compact sources at the OH position is less than or equal to 20 mJy at both frequencies.

[5] The OH 19.6−0.2 region has a complicated radio structure that is incompletely sampled by our observations. There are two nearly coincident compact components along the line of sight that are both optically thick at 2695 MHz.

[6] The source given in the table refers only to the most compact component present in the field. Most of the radio emission seen toward OH 34.3+0.2 (W44) at both frequencies arises in a very extended region that is incompletely sampled by our observations. Specifically, we see a maximum 2695 MHz fringe amplitude of 9.3 Jy arising in a $\theta \approx 60''$ region centered near $\alpha(1950) = 18^h50^m48\overset{s}{.}2$, $\delta(1950) = +01°10'47''$. For a more complete 2695 MHz continuum map of W44 one should refer to Turner *et al.* (1974).

[7] OH 35.2−1.7 is located $1\overset{s}{.}4$ west of the bright radio structure in W48. In addition to the components given in Table 2, we see a maximum fringe amplitude of 11 Jy emitted by a large 32″ × 58″ radio component located at $\alpha(1950) = 18^h59^m14\overset{s}{.}9$, $\delta(1950) = +01°08'31''$.

[8] In addition to the compact radio component given in the table, OH 35.6−0.0 coincides with a large, ~10′, low-surface-brightness H II region, the radio flux of which Altenhoff *et al.* (1970) find to be 15 Jy at 2695 MHz. We almost completely resolve this source; the maximum fringe amplitude at 1800λ is only 900 mJy.

[9] The extended radio component (*b*) seen at 2695 MHz is completely resolved at 8085 MHz.

data are often resolved out. This is evident most strikingly in OH 12.9−0.3, where a large, $\theta > 13''$, source is seen at 2695 MHz that contributes more than 5 Jy. On the longer 8085 MHz baselines, this source is so completely resolved that the maximum 8085 MHz fringe amplitude is less than 30 mJy. In cases like this, and especially for those OH emission sources seen toward known H II regions which have radio emission on a wide range of spatial scales (e.g., OH 34.3+0.2, OH 19.6−0.2), we have included a brief remark on their characteristics in the notes accompanying the table. Third, since many of the positions observed are either at large southern declinations or near zero declination, the (u, v) sampling is considerably more complete in one coordinate than in the other. Consequently, the parameters of the best-fit elliptical Gaussian components are better determined in one coordinate than in the other; for this reason, we tabulated source sizes in Table 4 that refer to the quadratic mean of the FWHM dimensions of the model sources. We estimate the uncertainty in the sizes so determined as about 20%. Finally, for those OH positions at which no coincident radio continuum source is seen, our upper limit to the emission from a compact source at the OH position is generally 15 mJy.

The detailed comparison of the component parameters at two frequencies is often misleading owing to the interaction between resolution and optical depth effects; this problem has been clearly illustrated by Balick (1972). The effect is present in our data and makes any determination of the physical parameters of the nebulae unreliable when it is derived solely from the data given in Table 4. In order to derive reliable parameters of the compact H II regions in Table 4, direct reference must be made to the visibility data.

In Figure 2, the ratio of the observed 8085 MHz fringe amplitude to the 2695 MHz fringe amplitude is plotted as a function of interferometer baseline b_λ. This plot is useful because the amplitude measured at each particular value of b_λ refers to emission from the same spatial structure at each frequency (Balick 1972); hence the uncertainties in modeling the sources are no longer present. In interpreting this figure, note the following: (1) If the only source present were unresolved and optically thin at both frequencies, then the fringe amplitude ratio would be 0.9 independent of b_λ. (2) If the source were unresolved and optically thick at both frequencies, the ratio would be 9 independent of b_λ. (3) If there exists both a large optically thin source and an unresolved optically thick source in the field, then the ratio will be 0.9 at small b_λ and increase toward 9 at large b_λ. The last case appears to describe five of the sources in Figure 2. The most important result seen in Figure 2 is that the compact radio sources which are coincident with the OH emission sources are *all* optically thick at 2695 MHz; that is, the fringe amplitude ratio on the longest baselines is greater than 0.9. For OH 34.4+0.2 and OH 43.8−0.1, the compact components are also optically thick at 8085 MHz. The sixth source, which is coincident with an OH emission source (OH 19.6−0.2), has a more complex structure (see notes to Table 4) but also has an optically thick component at 2695 MHz.

e) *Compact* H II *Regions and* OH *Masers*

Identifiable radio components are seen toward nine of the 10 OH emission sources as seen in Tables 1 and 4. The OH sources and compact H II regions are positionally coincident to within the uncertainties in

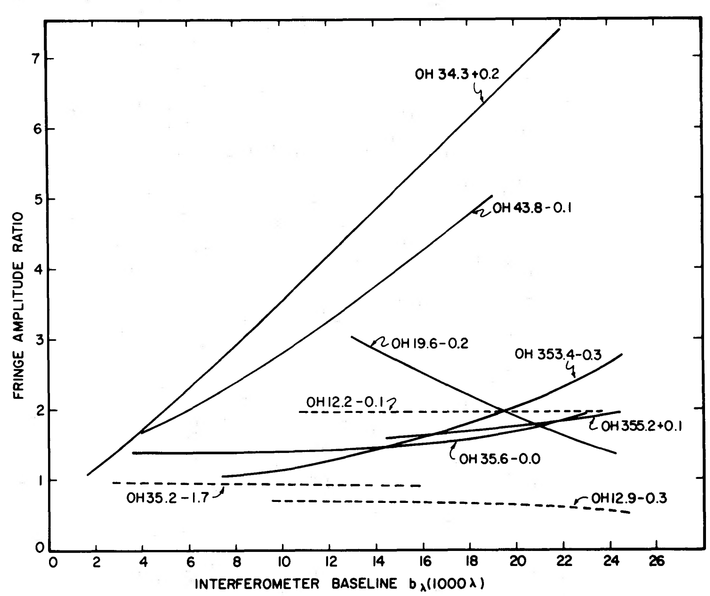

FIG. 2.—The ratio of the fringe amplitude at 8085 MHz to the fringe amplitude at 2695 MHz as a function of interferometer separation (in wavelengths) for the radio continuum sources seen toward the positions of the OH emission sources. The solid lines denote those radio sources that are coincident (within the errors) with the OH emission sources (Table 4), whereas the dashed lines are those sources for which the radio continuum does not peak at the OH emission position.

six of the nine fields. *In each of these six cases, the compact* H II *region coincident with the* OH *emission source is optically thick at 2695 MHz*. Hence the emission measure of each of these regions is at least as large as $2.5 \times 10^7 (T_e/10^4 \text{ K})^{-1.35}$ cm^{-6} pc and may be considerably larger than this value, particularly for the sources near OH 34.3+0.2 and OH 43.8−0.1. In two of the remaining three fields where the positions of the OH sources and compact H II regions are not coincident, the compact H II regions are not optically thick. OH 12.2−0.1 is the only field in which both an optically thick H II region and an OH emission source exist but do not coincide. With this single exception, there is good agreement between compact, optically thick H II regions and OH emission sources. OH 48.6+0.0 was not observed at NRAO, but 6 cm observations by Matthews *et al.* (1978) indicate that it is associated with a compact H II region. Matthews *et al.* (1978) also present data for sources near OH 43.8−0.1; they interpret the combination of their data with ours as indicating that two sources are present. One of these coincides with the OH position within the OH uncertainties.

f) Infrared Results

The positions and photometry of the infrared sources are given in Table 5. Dyck and Simon (1977) discovered two of the sources (IR 12.9−0.3 and IR 35.2−1.7) in connection with a study similar to ours. We measured several of the sources at four different times between 1974 and 1977; no significant temporal variations were observed. All sources except IR 40.6−0.1 and NGC 2071 IR were observed more than once. The lack of variability in the detected sources indicates that our failure to detect the other sources was not due to temporal variations.

We have searched for 10 μm emission from two of the four OH masers listed by Wynn-Williams and Becklin (1974) as having no infrared, W3(cont)OH and W51(OH). An infrared source was detected at the position of W3(cont)OH, but not at the position of W51(OH). In addition, an improved position for the W75N maser (Evans, Crutcher, and Wilson 1976) confirmed that the OH maser does not coincide with the H II region and infrared source studied by Wynn-Williams, Becklin, and Neugebauer (1974) but does coincide with a weaker H II region (Habing *et al.* 1974). We have searched without success for infrared emission at this position (see Table 5). The NGC 7538(S) OH maser was also rechecked for infrared emission by Wynn-Williams (private communication), who places a limit of 0.15 Jy at 10 μm.

The energy distributions are presented in Figure 3 for the four sources for which data exist over a significant range of wavelengths. Two of these sources show marginal evidence for a 9.5 μm absorption feature, which is commonly attributed to silicates. One

TABLE 5

Infrared Photometry*

Source (1)	α(1950) (2)	δ(1950) (3)	2.2μm (4)	3.4μm (5)	4.8μm (6)	8.7μm (7)	9.5μm (8)	10.1μm (9)	11.2μm (10)	12.5μm (11)	20μm (12)
IR12.2-0.1	-	-						<0.5+			
IR12.9-0.3**	$18^h11^m44^s.3$±4"	-17°53'02"±4"	.18±.03	2.7±.6	29±3	8±1	8±.2	9±1	5.5±.5	22±3	50±20
IR34.3+0.2	18 50 46.3±4	+01 11 12±4	<0.006	.07±.02	4.7±.8	3.8±.6	<0.7	4.1±.7	1.2±.4	12±2	6.4±35
IR35.2-1.7++	18 59 13.6±4	+01 09 01±4			1.7±.6	8±1	8±2	17±2	17±2	38±5	100±30
IR35.6-0.0	18 53 51.7±6	+02 16 30±6			<1.7			0.9±0.2			
IR40.6-0.1	19 03 35.5±6	+06 41 56±6						0.9±2.0			
IR43.8-0.1	-	-						<1.2			
IR48.6+0.0	-	-						<1.3			
W51(OH)IR	-	-						<1			
W75N(OH)IR	-	-						<1			
NGC7538(OH)S	-	-						<0.15+*			
W3(CONT)OHIR	02 21 46.5±6	+61 52 22±6		<.07	<0.8			1.0±0.2		2.0±0.5	25±10
NGC2071IR	05 44 30.2±4	+00 20 42±4		<1	6±1	7±1	5.5±1	15±2	15±2	34±5	80±18

*All photometric results are given in Jy; 1σ errors are indicated.

+All upper limits are 3σ

**A flux of 0.004±0.002 Jy has been measured for this source at 1.6μm; Dyck and Simon (1977) have detected this source at 25 and 33μm.

++The infrared source is south and east of the OH position (see also Dyck and Simon 1977 and Zeilik and Lada 1978); S_ν(10μm) < 3 Jy at the OH position.

+*Wynn-Williams, private communication.

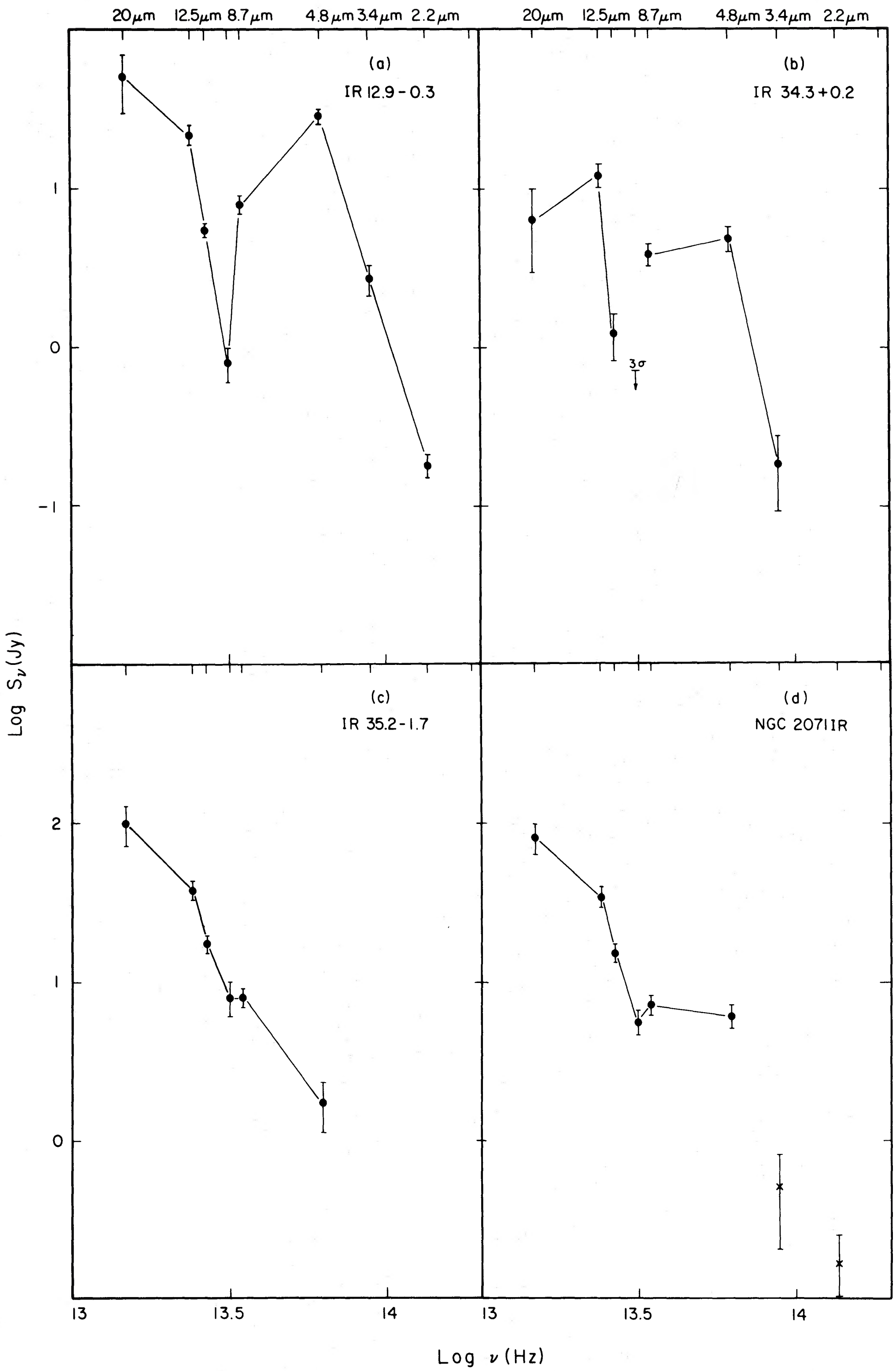

FIG. 3.—Infrared energy distributions of four infrared sources. For NGC 2071, the two data points marked with a cross were determined with a 30″ aperture at Kitt Peak National Observatory. Notice that the vertical scales are different for Figs. 3*a* and 3*b*, compared with 3*c* and 3*d*.

of these sources is IR 35.2−1.7, which coincides with an H II region but not with the OH source (cf. Tables 1 and 4). This region has been studied recently by Zeilik and Lada (1978); the OH position lies at the edge of their map of extended emission at 3.5 μm. The near-infrared power-law spectrum seen in this source is often observed in dust-embedded H II regions and has been interpreted as being due to emission at a range of dust temperatures (Scoville and Kwan 1976). The other infrared source, NGC 2071 IR, coincides with the OH position (Winnberg 1976; Johansson *et al.* 1974) within the fairly large uncertainties in the OH position, but no radio continuum from this direction has been found to a limit of 20 mJy at 2.8 cm (Johansson *et al.* 1974).

The other two sources in Figure 3, IR 12.9−0.3 and IR 34.3+0.2, exhibit deep absorption features at 9.5 μm and nearly equal fluxes at 4.8 and 20 μm. These properties are similar to those of objects found in molecular clouds at the positions of peaks in CO emission (e.g., Evans, Blair, and Beckwith 1977). For both these sources, the infrared position agrees well with the OH position (Fig. 4). One source (IR 34.3+0.2) also agrees with the position of an 8085 MHz source, while the other (IR 12.9−0.3) shows no compact radio source. The optical depth of the silicate feature in IR 12.9−0.3 is 3.4, as determined by interpolating between the 4.8 μm and 12.5 μm points to obtain a background flux, and by assuming the absorption arises in a uniform, cold layer that produces no emission itself.

IV. CORRELATIONS BETWEEN OH MASERS AND COMPACT H II REGIONS, INFRARED SOURCES, OR H_2O MASERS

Because the sources of energy for the maser pump are not known, early workers have studied the spatial correlations of OH masers with other luminosity sources. The work of Habing *et al.* (1974) has suggested a correlation between type I OH masers and compact H II regions. Wynn-Williams and Becklin (1974) have studied the correlation of OH masers and infrared sources. They did not find a strong correlation between these sources. Also, Hefele, Wacker, and Weinberger (1977) detected infrared sources at the positions of only one or two OH masers out of a sample of six. A study by Johnston, Sloanaker, and Bologna (1973) found H_2O masers toward half the type I OH masers searched; considering possible time variations, they suggested a one-to-one correlation between H_2O and type I OH masers. In this section, we will consider these correlations, using the data presented in this paper. The conclusions which result from the correlations in our sample are different than those of early samples. In particular, the results indicate that the study of correlations is probably not a good way of determining the nature of the pump.

The data in this study are more homogeneous than those of earlier studies; the upper limits in the case of nondetections were all obtained in the same way and the criteria for coincidence are well defined. Furthermore, this sample of OH masers is not subject to the

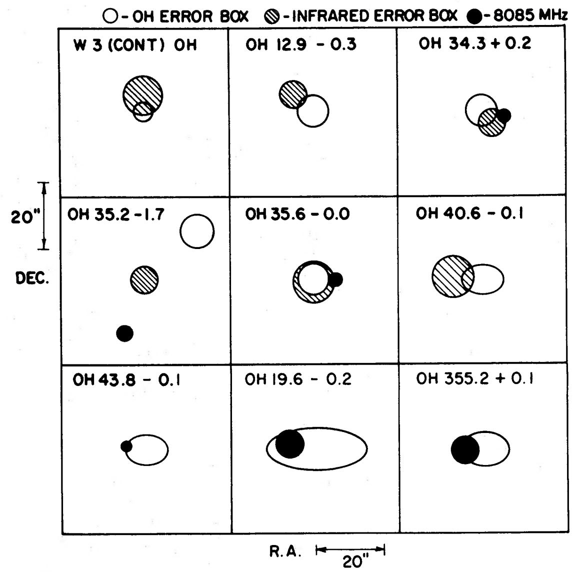

FIG. 4.—The positions and uncertainty ellipses for the OH masers, compact H II regions, and infrared sources.

same biases as previous samples, since the masers were found from a uniformly surveyed area (Turner 1978).

Our coincidence criteria are defined as follows: In the case of the radio continuum, we require that a compact source at 8085 MHz coincide with the OH position within the uncertainties. This criterion is used in Table 4. The four noncoincidences are all unambiguous, since two are well separated and the other two have no compact sources in the field (see Fig. 4). For infrared coincidence, we require that the infrared and OH positions coincide within the combined uncertainties; again there is no ambiguity. It should be noted, however, that infrared data are not available for all of the OH sources in the sample. For an H_2O maser to be considered coincident with an OH maser, we also require that the positions coincide to within the combined uncertainties. Since the positions of the H_2O masers are typically uncertain within ~1'.5, the coincidence requirement is much less stringent than for the first two cases.

Table 6 summarizes the spatial correlations for the OH masers with new positions. The resulting fractions which show a correlation with the OH sources are 0.64 for compact H II regions, 0.50 for the infrared sources, and 1.0 for the H_2O sources. The high correlation for H_2O sources may be due to the lack of accurate H_2O positions. There are a substantial number of OH masers where no compact H II region or infrared source exists. This result may be due to insufficient sensitivity; however, there exist OH masers with infrared sources but without compact H II regions and also OH masers with compact H II regions but without infrared sources. The evidence from this study for a correlation between OH masers and infrared sources is about as strong as that for a correlation between OH masers and compact H II regions.

TABLE 6

CORRELATIONS: SOURCES WITH NEW POSITIONS

OH Source (1)	Compact H II Region (2)	Position Difference* (3)	Infrared Source (4)	Position Difference+ (5)	H_2O Maser (6)
OH353.4-0.3	Yes	8"±15"	-	-	-
OH355.2+0.1	Yes	7±10	-	-	-
OH12.2-0.1	No	65±8	No	-	Yes
OH12.9-0.3	No	-	Yes	8"±9"	Yes
OH19.6-0.2	Yes	8±17	-	-	Yes
OH34.3+0.2	Yes	8±7	Yes	5±9	Yes
OH35.2-1.7	No	38±7	No	22±9	Yes
OH35.6-0.0	Yes	6±7	Yes	1±11	Yes
OH40.6-0.1	No	-	Yes	9±12	Yes
OH43.8-0.1	Yes	6±9	No	-	Yes
OH48.6+0.0	Yes**	4±7	No	-	Yes

*Errors are $(\sigma_\alpha^2(\mathrm{OH}) + \sigma_\delta^2(\mathrm{OH}))^{0.5}$; radio continuum position errors are negligible.

+Errors are $(\sigma_\alpha^2(\mathrm{OH}) + \sigma_\delta^2(\mathrm{OH}) + \sigma_\alpha^2(\mathrm{IR}) + \sigma_\delta^2(\mathrm{IR}))^{0.5}$

**Matthews et al. (1978)

These results may be compared with the results of earlier studies. In Table 7, an updated version of Table 2 of Wynn-Williams and Becklin (1974) is presented. Several objects with large OH position uncertainties or no OH emission have been left out. NGC 2071 and S255 have been added to the table. Although the data are quite inhomogeneous, it is interesting to note that the fractions of OH masers which have associated radio emission, infrared sources, or H_2O masers are 0.57, 0.71, and 0.57, respectively. Thus, for this sample, the correlation of OH masers with H II regions or with H_2O masers is weaker than the correlation with infrared sources. Since most of these OH masers were found by looking at known H II regions, the sample would normally be biased toward a correlation between OH masers and H II regions. Furthermore, the requirements for a coincidence of an infrared source and OH maser are more stringent than for the coincidence of OH with a radio continuum source. In the case of W51, for example, the OH source is located just off the edge of the radio continuum and 20 μm contours (Wynn-Williams, Becklin, and Neugebauer 1974); the radio continuum is considered coincident because OH masers are commonly found at the edge of H II regions (Habing *et al.* 1974); but the infrared source is not considered coincident.

From the above discussion of correlations, we conclude that Type I OH masers are equally likely to be associated with infrared sources as with compact H II regions. This conclusion may differ from that of other workers because of the detection of several sources at levels below the sensitivity limits of previous studies. For example, the upper limits at 10.7 μm presented by Hefele, Wacker, and Weinberger (1977) are ~3–6 Jy; only half the sources in Table 5 lie above this limit. As positions and sensitivities improve, the correlations continue to change; it is not yet clear what the final picture will be. For example, the strong correlation between OH and H_2O masers found in our study is very likely due to the large uncertainties in the H_2O maser positions. Some support for this statement may be found from studies of other sources. Recently, accurate (±0''.5) positions for 10 H_2O masers were obtained by Forster *et al.* (1978); only six were coincident with OH masers. While the results of Forster *et al.* (1978) bear principally on the nature of the H_2O masers, they also suggest that more accurate OH positions are needed to settle the issue of OH maser correlations. We conclude that the common presence of OH and H_2O masers, compact H II regions, and infrared sources in the same *general* area is indicative of ongoing star formation, but that statements about the *detailed* associations of OH masers with the other objects cannot yet be made.

V. PUMPING MODELS

If one attempted to understand the pumping process through a study of the correlations discussed above, one would be tempted to conclude that the H_2O masers pump the OH masers. In this case, the study of correlations is not a reliable way to assess causal relationships. Instead, specific pumping mechanisms must be tested against observations. We consider below some pump-

TABLE 7

CORRELATIONS: PREVIOUSLY STUDIED SOURCES

OH Source (1)	H II Region (2)	Infrared Source (3)	Position Difference (4)	H_2O Maser (5)	References (6)
W3(OH)	Yes	Yes	2"±3"	No*	1
W3(CONT)OH	No	Yes*	5±7	No	
Orion (KL)	No	Yes	<5"	Yes	
S269	Yes	Yes	7±10	Yes	
W49(1)	Yes	Yes	3±5	Yes	
W49(2)	Yes	Yes	5±5	Yes	
W51	Yes*	No**		No*	2
OH1959+33	Yes	No		No	
W75(S)	No	Yes	≤5	No*	2
W75(N)	Yes+	No+		Yes	
NGC7538(OH)N	Yes	Yes	1±3	No*	
NGC7538(OH)S	No	No		Yes*	2
NGC2071	No	Yes	12±19	Yes	3, 4
S255	No	Yes	7±23	Yes	5

*Note change from Table II of Wynn-Williams and Becklin (1974)

+New data (Evans, Crutcher, and Wilson 1976) indicate the OH maser does not coincide with the H II/IR source of Wynn-Williams et al. (1974), but does coincide with a weaker H II region (Habing et al. 1974).

**New search was made as shown in Table 5.

1. Forster et al. 1977
2. Forster et al. 1978
3. Johansson et al. 1974
4. Winnberg, private communication
5. Evans, Blair, and Beckwith, 1977

ing models which have been proposed. Even though some of these models can be shown not to apply to specific cases (cf. Elitzur and de Jong 1978), a re-examination of the question for this sample is of value because different pumping models may apply for different sources.

a) *Ultraviolet Pumping*

Litvak *et al.* (1966) suggested that OH masers may be pumped by ultraviolet photons at 3060–3080 Å. The radio continuum data presented in Table 4 provide us with a means of estimating the rate at which the OH masers presented here may be pumped by ultraviolet photons. For a given spectral type, the flux of Lyman-continuum photons ϕ_L can be related to the flux of photons at the pumping wavelength (ϕ_p). If the relationship given by Matsakis *et al.* (1976) for ϕ_L is used and we assume that the H II regions are optically thin at 8085 MHz, then $\phi_p = 9.2 \times 10^{46}\chi(T_{\rm eff}, R_*)S_\nu D^2 f_{\rm abs}$ photons s^{-1}. Here D is the distance to the source in kpc, S_ν is the flux in Jy at 8085 MHz, $\chi(T_{\rm eff}, R_*)$ is the ratio of pumping photons to Lyman-continuum photons produced by a blackbody of radius R_* and temperature $T_{\rm eff}$, and $f_{\rm abs}$ is the fraction of the pumping photons absorbed by the maser region. This should be compared with the number of OH maser photons s^{-1}, $\phi_{\rm OH} = 9.5 \times 10^{12} S_\nu({\rm OH})\delta\nu_{\rm OH} D^2 \Omega_{\rm em}(h\nu_{\rm OH})^{-1}$ photons s^{-1}, where S_ν(OH) is the flux in Jy in the maser line of width $\delta\nu_{\rm OH}$, $h\nu_{\rm OH}$ is in joules, and $\Omega_{\rm em}$ is the solid angle into which the OH maser emits. Because there are six ultraviolet lines that provide pumping, the pump efficiency is $\phi_{\rm OH}/6\phi_p$. The quantity $\chi(T_{\rm eff}, R_*)$ increases rapidly for stars of later spectral class: for B0 stars $\chi = 1.5 \times 10^{-14}\delta\nu$, where $\delta\nu$ is the bandwidth over which the OH absorbs the pumping photons; in the case of a B1 star, $\chi = 6.9 \times 10^{-13}\delta\nu$. Since the detected H II regions require stars of spectral type earlier than ~B0 at the near kinematic distance, a generous limit for χ is $\chi < 10^{-12}\delta\nu$. If the Doppler motions of the OH molecules determine both the absorption and emission bandwidth, then the resulting efficiency is

$$\frac{\phi_{\rm OH}}{6\phi_p} = 3 \times 10^{-4}\frac{S_\nu({\rm OH})}{S_\nu}\frac{\Omega_{\rm em}}{4\pi}\frac{1}{f_{\rm abs}}\,.$$

If we take the results from Tables 2 and 4, and assume

$\Omega_{em} = 4\pi$ and $f_{abs} = 1$, we find efficiencies ranging from 0.027 to more than 3.8, the latter corresponding to the upper limits at 8085 MHz on OH 40.6−0.1 and OH 12.9−0.3. Holtz (1968) has shown that the efficiency of the ultraviolet pump can be no greater than 0.01. None of the sources satisfy this condition; to bring OH 40.6−0.1 and OH 12.9−0.3 into agreement with this figure, $\Omega_{em}/4\pi$ would have to be less than 3×10^{-3}. Furthermore, we have assumed that all the ultraviolet photons get absorbed by the OH. The fact that many OH masers come from small sources on the side of H II regions suggests that f_{abs} is small. Finally, the OH molecules must be selectively shielded from the shorter-wavelength ultraviolet which will dissociate them.

b) *Far-Infrared Pumping*

A second pumping model involves far-infrared radiation. First discussed by Litvak (1969), this pumping model is usually applied to the satellite line inversions, but it has recently been reevaluated by several workers (Burdyuzha and Varshalovich 1973; Elitzur 1978*a*), who find that certain conditions give rise to main-line inversions. In addition, Burdyuzha (1973) has proposed a mechanism for selecting the 1665 MHz line through 35 μm photons after having inverted the Λ doublet with 53 μm radiation. The mechanisms require radiation from dust at temperatures around 100 K. While Elitzur applies his model only to the main-line masers associated with OH/IR stars, Burdyuzha and Varshalovich propose their mechanism as an explanation for masers of the type discussed in this paper.

The pumping efficiency is

$$\frac{\phi_{OH}}{\phi_p} = \frac{S_\nu(\mathrm{OH})}{S_\nu(\mathrm{FIR})}\left(\frac{\Omega_{em}}{4\pi}\right)\left(\frac{1}{f_{abs}}\right).$$

Unfortunately, we have no direct measurement of the fluxes at the wavelengths at which the pumps operate. Because the pumping models seem to require $T_d \sim$ 100 K, we have used a color temperature of 100 K to estimate the fluxes at 35 and 53 μm from the 10 and 20 μm data. This procedure is at best very crude and it demonstrates that far-infrared observations would be useful. The resulting efficiencies range from 0.10 to 5, with most of the estimates at $\sim$0.5. The fraction of absorbed pumping photons, f_{abs}, is probably much less than 1, as in the case of the ultraviolet pumping. In this case, f_{abs} is low because the OH maser region would be embedded in a much larger far-infrared emitting region. In this situation $f_{abs} \sim (R_{OH}/R_{FIR})^2$, where R_{OH} and R_{FIR} are the sizes of the OH and far-infrared emitting regions. Thus, for far-infrared pumping, as well as for ultraviolet pumping, the solid angle of maser emission would have to be considerably less than 4π.

c) *Collisional Pumping*

Various chemical and collisional pumping models have been considered (Gwinn *et al.* 1973; Bertojo, Cheung, and Townes 1976), but our data do not bear directly on most of these models. Our observations do provide a test of one collisional model. A collisional pump involving anisotropic streams of electrons was proposed by Johnston (1967) and has been reexamined by Elitzur (1978*b*), who considered the effects of streaming ions as well as electrons. Elitzur (1978*b*) found that ions could readily acquire an anisotropic velocity distribution because of ambipolar diffusion, but available calculations of ion-molecule collision rates are not capable of establishing that these collisions will invert the OH maser levels. In contrast, collisions with anisotropic electrons will produce the inversion, but the method for producing the streams is not established. In Elitzur's model, the masers arise in compressed gas between the shock and ionization fronts of an expanding H II region. This model produces maser amplification only in directions orthogonal to the streaming direction of the particles. Each maser spot is associated with a cylinder which is perpendicular to the radius vector of the H II region. A natural consequence of the model in its simplest form is the production of linear polarization in the maser radiation. A mechanism to convert linear to circular polarization is then required to explain the large circular polarization observed in many masers. If the mechanism is associated with turbulence, which also produces multiple velocity features, then one would expect that the sources with only a few velocity components would show more linear polarization. This expectation is in general agreement with our polarization results.

Elitzur (1978*b*) presents formulae for calculating the flux of maser photons predicted by a model in which electrons have acquired a streaming velocity of 40 km s^{-1}. These formulae are used to compute the maser flux predicted for the sources where we have observed compact H II regions at 8085 MHz. The predictions will then be compared with the observed fluxes. Rewriting equation (31) of Elitzur in a form suitable to this purpose, we obtain, for the predicted flux of maser photons,

$$\phi_p = 1.57 \times 10^{-14} n_I^{3-2\kappa} R^2 d,$$

where n_I (cm^{-3}) is the initial unshocked density, κ determines the original, unshocked magnetic field through $B = 3 \times 10^{-6} n^\kappa$, R (cm) is the radius of the H II region, d is the distance between the shock and ionization fronts (and also the maser spot size). In the derivation of the expression, it is assumed that the original density in the unshocked neutral gas has been increased to $n = 0.31 V_s n_I^{(3/2-\kappa)}$ (eq. [12] of Elitzur), where $V_s = 15$ km s^{-1} is the shock velocity. The equation for ϕ_p also depends on assuming $n_{OH} = 2 \times 10^{-4} n$ and a fractional ionization of 10^{-5}, which result from chemical and ionization models of the maser region by Elitzur and de Jong (1978).

Elitzur (1978*b*) has restricted κ to the range $\frac{1}{3}$ to $\frac{1}{2}$, on the basis of work by Mouschovias (1976). By considering the role of κ in the above equation, one concludes that ϕ_p is maximized by taking κ at the low end of its range, $\kappa = \frac{1}{3}$. In the calculation of ϕ_p, we have used $\kappa = \frac{1}{3}$. The radius of the H II region (R) was determined from the angular size of the 8085 MHz source (Table 4) and a kinematic distance (D) to the source. The original unshocked density (n_{I}) will equal the present electron density (n_e) if the H II region has not begun to expand. More generally $n_{\mathrm{I}} \geq n_e$; consequently, the substitution of $n_e = n_{\mathrm{I}}$ will lead to a lower limit for ϕ_p. The electron density was determined from the 8085 MHz observations and the relation given by Matsakis *et al.* (1976). The maser spot size is not known in these sources, since VLBI experiments have not been made; we assume $d = 0.01R$, based on analogy with W3(OH) and on some theoretical support (Elitzur 1978*b*). The values of D, R, n_e, ϕ_p, and ϕ_o (the observed flux) are presented in Table 8. Isotropic emission has been assumed in computing the predicted and observed fluxes.

As can be seen from Table 8, the predicted flux exceeds the observed flux for every source except OH 43.8−0.1, where $\phi_p \sim 0.3\phi_o$. A solid angle of emission, $\Omega_{\mathrm{em}} \sim \pi$, could account for such a discrepancy. In addition, the electron density in this source could be seriously underestimated because the H II region appears to be optically thick at 8085 MHz. It should be noted that the use of a kinematic distance does not introduce significant error, because ϕ_p and ϕ_o depend on distance in nearly the same way. The major uncertainty with this model is that the mechanism for producing the streaming electrons is unknown, and ϕ_p is proportional to the streaming velocity. Elitzur (1978*b*) *assumes* that this velocity is equal to the thermal velocities ($\sim$40 km s^{-1}); even a velocity 10 times less than this would give $\phi_p > \phi_o$ in all but the last two sources in Table 8. If a mechanism for accelerating the electrons can be found, or if ion collisions can be shown to invert the OH, then this pumping model would be quite attractive.

VI. SUMMARY

Accurate positions have been measured for 11 type I OH masers. We have determined the Stokes parameters of the OH emission and find that several of the sources exhibit considerable linear polarization. There appears to be an anticorrelation between the number of velocity components and the fraction of linear polarization. The predominance of circular polarization in previously studied masers is contrasted with this result; further study of the "simple" sources may determine the polarization mechanism.

H_2O maser emission was detected toward all eight of the OH sources which were observed at the H_2O frequency. Some of these sources were detected in other studies. The positions of the H_2O sources are not sufficiently accurate for detailed spatial comparison with the OH masers.

The radio continuum emission in the direction of 10 of the OH masers was studied at 2695 and 8085 MHz. In six cases, a compact H II region which is optically thick at 2695 MHz is coincident with the source. In three cases, no compact H II region which is optically thick at 2695 MHz exists in the field (6′ diameter at 8085 MHz). In only one case does such a compact H II region exist within the field but not coincide with the OH position.

Infrared observations were obtained in the direction of eight of the OH sources with position measurements. Four of the eight OH sources have infrared sources at the same positions. Two of these sources were detected only at 10 μm. For the other two sources, data were taken from 2 to 20 μm; both sources show deep absorption features at 9.5 μm. In addition, infrared sources were detected at the positions of W3(cont)OH and the

TABLE 8

H II REGION PARAMETERS AND FLUXES PREDICTED FROM ANISOTROPIC COLLISIONS WITH CHARGED PARTICLES

OH Source (1)	D (kpc) (2)	R (cm) (3)	n_e (cm^{-3}) (4)	ϕ_P (s^{-1}) (5)	ϕ_o (s^{-1}) (6)
OH353.4-0.3	3.8	7.0×10^{16}	5.0×10^{4}	5.0×10^{45}	1.6×10^{43}
	14.6	2.7×10^{17}	2.5×10^{4}	5.7×10^{46}	2.4×10^{44}
OH355.2+0.1	-	-	-		-
	24.4	7.5×10^{17}	8.4×10^{3}	9.5×10^{46}	2.7×10^{45}
OH19.6-0.2	3.8	1.0×10^{17}	2.8×10^{4}	3.7×10^{45}	1.3×10^{43}
	15.1	4.0×10^{17}	1.4×10^{4}	4.8×10^{46}	2.1×10^{44}
OH34.3+0.2	4.1	4.8×10^{16}	1.2×10^{5}	1.2×10^{46}	4.3×10^{44}
	12.6	1.5×10^{17}	6.9×10^{4}	1.0×10^{47}	4.0×10^{45}
OH35.6-0.0	3.4	4.8×10^{16}	3.2×10^{4}	5.6×10^{44}	2.8×10^{44}
	13.3	1.9×10^{17}	1.6×10^{4}	7.0×10^{45}	4.3×10^{45}
OH43.8-0.1	2.7	2.0×10^{16}	6.2×10^{4}	1.9×10^{44}	5.1×10^{44}
	11.8	9.0×10^{16}	3.0×10^{4}	3.2×10^{45}	9.7×10^{45}

OH maser near NGC 2071; both of these sources are extremely red. Upper limits were obtained at 10 μm at the positions of three other OH masers.

We have reexamined the correlations between OH masers and compact H II regions, infrared sources, and H_2O masers, both for the sources whose positions are reported here and for a group of previously studied sources. The strongest correlation in both groups is between OH and H_2O masers, but this effect may be due to the large uncertainties in the H_2O maser positions. While positive correlations exist between OH masers and compact H II regions and between OH masers and infrared sources, there are a substantial number of OH masers where no compact H II region or infrared source exists. This may be due to the sensitivity limits of both the radio continuum and infrared searches. Overall, the evidence for a correlation between infrared sources and OH masers is about as strong as that for a correlation between compact H II regions and OH masers. These results, when contrasted with earlier correlation studies, indicate that a study of correlations is not a particularly good way to determine the pumping mechanism.

On the basis of our measurements of the total OH maser flux and the measurements of continuum flux at 8085 MHz, we have considered the feasibility of ultraviolet pumping of these masers. Our data indicate that quite generous assumptions have to be made in order to predict enough ultraviolet pumping photons to produce the observed flux of OH maser photons.

Pumping by far-infrared photons at 53 and 35 μm was considered in view of our infrared measurements and an assumed dust temperature of 100 K; the latter is required by the far-infrared pumping models. For this pump rather generous assumptions are required to make the pump efficiency less than unity.

Finally, pumping by anisotropic collisions with ions or electrons streaming through the neutral gas was considered. The fluxes of maser photons predicted by a model assuming electron streaming at 40 km s^{-1} are sufficient to explain the observed maser flux in all but one of our sources. The one exception can be readily accounted for by plausible uncertainties. Because no mechanism for producing the streaming electrons has been established, this model remains incomplete. If such a mechanism can be found, or if ion collisions can be shown to invert the OH, then this model would become quite attractive.

We wish to thank the staffs of Owens Valley Radio Observatory, Mount Wilson Observatory, and the National Radio Astronomy Observatory for making these observations possible. C. Spencer and H. Hardebeck provided invaluable assistance with the receivers and M. Cimerman, K. Y. Lo, and G. Knapp provided some of the observations at OVRO. H. Lanning, J. Frazier, and D. Nadeau provided assistance at Mount Wilson. We wish to thank G. Neugebauer for the use of infrared equipment while observing at Mount Wilson. B. Zuckerman assisted with the observations at NRAO. We wish to thank B. Turner for providing the results of his OH survey. H. Matthews, W. M. Goss, and P. Shaver provided data in advance of publication. At various stages of this project, helpful discussions were provided by E. Becklin, P. Goldreich, and G. Neugebauer. Research at Owens Valley Radio Observatory is supported by the National Science Foundation under MPS 73-004677A2 and by the Office of Naval Research under contract N00014-67-A-0094-0019. This work was supported in part by National Science Foundation grants AST 75-22903 and AST 74-18555A2 and by National Aeronautics and Space Administration grants NGL 05-002-207 and NSG-7381.

REFERENCES

Altenhoff, W. J., Downes, D., Goad, L., Maxwell, A., and Rinehart, R. 1970, *Astr. Ap. Suppl.*, **1**, 319.
Balick, B. 1972, *Ap. J.*, **176**, 353.
Beckwith, S., Evans, N. J., II, Becklin, E. E., and Neugebauer, G. 1976, *Ap. J.*, **208**, 390.
Bertojo, M., Cheung, A. C., and Townes, C. H. 1976, *Ap. J.*, **208**, 914.
Burdyuzha, V. V. 1973, *Ap. Letters*, **15**, 189.
Burdyuzha, V. V., and Varshalovich, D. A. 1973, *Astr. Zh. USSR*, **50**, 481.
Caswell, J. A., Batchelor, R. A., Haynes, R. F., and Huchtmeier, W. K. 1974, *Australian J. Phys.*, **27**, 417.
Caswell, J. L., and Robinson, B. J. 1974, *Australian J. Phys.*, **27**, 629–635.
Dickinson, D. F., and Turner, B. E. 1972, *Ap. Letters*, **11**, 1–5.
Downes, D. 1970, *Ap. Letters*, **5**, 53.
Dyck, H. M., and Simon, T. 1977, *Ap. J.*, **211**, 421.
Elitzur, M. 1978*a*, *Astr. Ap.*, **62**, 305.
———. 1978*b*, *Astr. Ap.*, in press.
Elitzur, M., and de Jong, T. 1978, *Astr. Ap.*, in press.
Evans, N. J., II, Blair, G. N., and Beckwith, S. 1977, *Ap. J.*, **217**, 448.
Evans, N. J., II, Crutcher, R. M., and Wilson, W. J. 1976, *Ap. J.*, **206**, 440.
Forster, J. R., Welch, W. J., and Wright, M. C. H. 1977, *Ap. J. (Letters)*, **215**, L121.
Forster, J. R., Welch, W. J., Wright, M. C. H., and Baudry, A. 1978, *Ap. J.*, **221**, 137.
Goss, W. M., Lockhart, I. A., Fomalont, E. B., and Hardebeck, E. G. 1973, *Ap. J.*, **183**, 843–850.
Gwinn, W. D., Turner, B. E., Goss, W. M., and Blackman, G. L. 1973, *Ap. J.*, **179**, 789.
Habing, H. J., Goss, W. M., Matthews, H. E., and Winnberg, A. 1974, *Astr. Ap.*, **35**, 1–5.
Hefele, H., Wacker, W., and Weinberger, R. 1977, *Astr. Ap.*, **56**, 407.
Holtz, J. Z. 1968, *Ap. J. (Letters)*, **153**, L117.
Johansson, L. E. B., Höglund, B., Winnberg, A., Nguyen-Quang-Rieu, and Goss, W. M. 1974, *Ap. J.*, **189**, 455.
Johnston, I. D. 1967, *Ap. J.*, **150**, 33.
Johnston, K. J., Sloanaker, R. M., and Bologna, J. M. 1973, *Ap. J.*, **182**, 67.
Litvak, M. M., McWhorter, A. L., Meeks, M. L., Zeiger, H. J. 1966, *Phys. Rev. Letters*, **17**, 821.
Litvak, M. M. 1969, *Ap. J.*, **156**, 471.
Matsakis, D. N., Evans, N. J., II, Sato, T., and Zuckerman, B. 1976, *A.J.*, **81**, 172.
Matthews, H. E., Shaver, P. A., Goss, W. M., and Habing, H. J. 1978, *Astr. Ap.*, **63**, 307.
Mouschovias, T. Ch. 1976, *Ap. J.*, **207**, 141.
Palmer, P., and Zuckerman, B. 1967, *Ap. J.*, **148**, 727.
Robinson, B. J., Caswell, J. L., and Goss, W. M. 1971, *Ap. Letters*, **9**, 5.
Scoville, N. Z., and Kwan, J. 1976, *Ap. J.*, **206**, 718.
Shaver, P. A., and Danks, A. C. 1978, *Astr. Ap.*, **65**, 323.
Turner, B. E. 1970*a*, *J.R.A.S. Canada*, **64**, 221.

Turner, B. E. 1970*b*, *Ap. Letters*, **6**, 99.
———. 1978, *Astr. Ap. Suppl.*, submitted.
Turner, B. E., Balick, B., Cudaback, D. D., Heiles, C., and Boyle, R. J. 1974, *Ap. J.*, **194**, 279.
Turner, B. E., and Rubin, R. H. 1971, *Ap. J.* (*Letters*), **170**, L113.
Winnberg, A. 1976, unpublished data.
Winnberg, A., Nguyen-Quang-Rieu, Johansson, L. E. B., and Goss, W. M. 1975, *Astr. Ap.*, **38**, 145.
Wynn-Williams, C. G., and Becklin, E. E. 1974, *Pub. A.S.P.*, **86**, 509.
Wynn-Williams, C. G., Becklin, E. E., and Neugebauer, G. 1974, *Ap. J.*, **187**, 473.
Wynn-Williams, C. G., Werner, M. W., and Wilson, W. J. 1974, *Ap. J.*, **187**, 41.
Zeilik, M., II, and Lada, C. J. 1978, *Ap. J.*, **222**, 896.

S. Beckwith: Astronomy Department, Cornell University, Space Science Bldg., Ithaca, NY 14853

Robert L. Brown: National Radio Astronomy Observatory, P.O. Box 2, Green Bank, WV 24944

Neal J. Evans II: Department of Astronomy, The University of Texas at Austin, Austin, TX 78712

W. Gilmore: Astronomy Department, University of Toronto, 60 St. George St., Toronto, ON M5S1A7, Canada